Publication Year	2019
Acceptance in OA	2021-02-12T16:04:48Z
Title	Orbit-Like Proton Radiation Sensitivity of CdTe Detectors: Evaluation of Mobility-Lifetime Products and Spectroscopic Properties
Authors	Pascoa, M. P., Maia, J. M., AURICCHIO, NATALIA, Curado da Silva, R. M., Crespo, P., do Carmo, S. J. C., Moita, M., Alves, F., CAROLI, EZIO
Publisher's version (DOI)	10.1109/TNS.2019.2935119
Handle	http://hdl.handle.net/20.500.12386/30370
Journal	IEEE TRANSACTIONS ON NUCLEAR SCIENCE
Volume	66

Orbit-Like Proton Radiation Sensitivity of CdTe Detectors: Evaluation of Mobility-Lifetime Products and Spectroscopic Properties

M. P. Páscoa, J. M. Maia, N. Auricchio, R. M. Curado da Silva, P. Crespo, S. J. C. do Carmo, M. Moita, F. Alves, and E. Caroli

***Abstract*— This article reports the proton radiation sensitivity of two 1.0-mm-thick EURORAD ohmic CdTe detectors, irradiated with a low energy proton beam generated in a positron emission tomography (PET) cyclotron facility. The CdTe crystals were exposed to a proton radiation field composed of energies of ≈13.8, ≈9.7, ≈5.7, and ≈3.3 MeV, at an average flux of $\sim 10^8$ protons $cm^{-2}s^{-1}$, a total fluence from $\approx 2.1 \times 10^9$ up to $\approx 4.5 \times 10^{10}$ protons cm^{-2}, and an average dose from ≈5.9 up to ≈130 Gy, equivalent to the proton fluence accumulated in ∼1 up to ∼20 years in a low earth orbit (LEO). The impact of the proton radiation field was analyzed through its charge transport properties—the mobility-lifetime product for electrons, $(\mu\tau)_e$, and holes, $(\mu\tau)_h$,—and spectroscopic properties—the energy resolution and the peak-to-valley ratio, for γ-ray lines within 60–662 keV. The tested CdTe detectors, with $(\mu\tau)_e \sim 5 \times 10^{-4}$ cm^2V^{-1} and $(\mu\tau)_h \sim 3 \times 10^{-5}$ cm^2 V^{-1}, showed good radiation hardness, with the measured upper-limit of $(\mu\tau)_e$ and $(\mu\tau)_h$ proton fluence (average dose) sensitivity of $\sim 2 \times 10^{-15}$ cm^2V^{-1}/protons cm^{-2} ($\sim 7 \times 10^{-7}$ cm^2 V^{-1}/Gy) and $\sim 3 \times 10^{-16}$ cm^2 V^{-1}/protons cm^{-2} ($\sim 1 \times 10^{-7}$ cm^2 V^{-1}/Gy), respectively. Up to ≈130 Gy, no significant degradation of the energy resolution and the peak-to-valley ratio was observed.**

***Index Terms*— CdTe detectors, gamma-ray detectors, mobility-lifetime products, proton damage, radiation hardness, space radiation.**

Manuscript received June 3, 2019; revised August 6, 2019; accepted August 10, 2019. Date of publication August 13, 2019; date of current version September 16, 2019. The work of M. Moita was supported by the Doctorate in Applied and Engineering Physics FCT through the Ph.D. Program, Portugal, under Grant PD/BD/105922/2014.

M. P. Páscoa, R. M. Curado da Silva, P. Crespo, and M. Moita are with the LIP–Laboratório de Instrumentação e Física Experimental de Partículas, 3004-516 Coimbra, Portugal, and also with the Department of Physics, University of Coimbra, 3004-516 Coimbra, Portugal (e-mail: marcelapascoa@hotmail.com; rui.silva@coimbra.lip.pt; crespo@lip.pt; miguel.moita@coimbra.lip.pt).

J. M. Maia is with the Department of Physics, University of Beira Interior (UBI), 6201-001 Covilhã, Portugal, and also with the LIP–Laboratório de Instrumentação e Física Experimental de Partículas, 3004-516 Coimbra, Portugal (e-mail: jmaia@ubi.pt).

N. Auricchio and E. Caroli are with the INAF–Osservatorio di Astrofisica e Scienza dello spazio (OAS) di Bologna, 40129 Bologna, Italy (e-mail: natalia.auricchio@inaf.it; ezio.caroli@inaf.it).

S. J. C. do Carmo is with the ICNAS–Produção, University of Coimbra, Pólo das Ciências da Saúde, Azinhaga de Santa Comba, 3000-548 Coimbra, Portugal (e-mail: sergiocarmo@uc.pt).

F. Alves is with the ICNAS–Instituto de Ciências Nucleares Aplicadas à Saúde, University of Coimbra, 3000-548 Coimbra, Portugal, and also with the IPC–Instituto Politécnico de Coimbra, Coimbra Health School, 3046-854 Coimbra, Portugal (e-mail: franciscoalves@uc.pt).

I. Introduction

ANALYSIS of potential effects of the orbital radiation environment on space instrumentation is essential to project a high-energy astrophysics space mission [1]–[5]. Inline, it is crucial to study detector materials' radiation damage and its effects on their operational performances under conditions that are as similar as possible to the ones existing in the orbital radiation environment. In any orbit, to foresee the operational performances and the expected lifetime of a detection device, it is critical to know the environment radiation type and profile. Semiconductor detection planes, particularly CdTe planes require further space equivalent radiation environment tests in order to improve the new instrument concepts' sensitivity in orbits, such as 3-D CZT/CdTe detection planes [6], [7] and Laue lens CZT/CdTe focal planes [8], [9] applied in γ-ray astrophysics.

Most of the scientific satellites in the hard X-ray and γ-ray domains are placed in low earth orbits (LEOs) at flight altitudes within 500 and 600 km and inclinations within 20° and 40°, e.g., satellites Fermi, SWIFT and RHESSI [10]–[12]. An exception is the INTEGRAL satellite that has a highly eccentric orbit [13]. Furthermore, nowadays popular low-cost space research solutions such as CubeSat constellations [14] are generally conceived for LEOs.

Nevertheless, most of the time, LEO satellites orbit below the inner proton belt over 700-km altitude. When crossing the South Atlantic Anomaly (SAA), they are exposed to high proton fluxes [15], [16]. For instance, a high-energy telescope on board of a satellite in a typical LEO, e.g., ≈550-km altitude and ≈30° inclination, thus with ≈96-min period, similar to the recently lost ASTRO-H satellite [17], is exposed to geo-magnetically trapped protons with energy within 1 and 300 MeV and a differential average flux within ≈2 and ≈0.03 protons cm^{-2} s^{-1} MeV^{-1}, yielding an overall integrated average flux of ≈70 protons cm^{-2} s^{-1}, when estimated using OMERE software [18].

A space telescope in a typical LEO crosses the SAA with an average frequency of ≈8 times per day, spending ∼20 min in each passage with an overall integrated flux with a maximum of $\approx 3 \times 10^3$ protons cm^{-2} s^{-1}. The differential and integrated average fluences for a 1-year mission are shown in Fig. 1 for an overall integrated average fluence of $\approx 2.1 \times 10^9$ protons cm^{-2}.

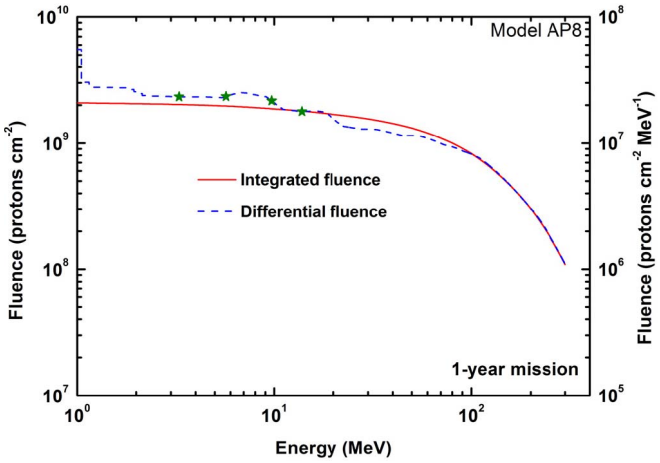

Fig. 1. Trapped proton integrated and differential average fluence for a 1-year mission in a LEO—≈550-km altitude, ≈30° inclination, and ≈96-min period, up to 300 MeV, calculated using OMERE v4.2 software [18] for the AP8-MIN model. The fluence is omnidirectional: 4π sr. The closed symbols show the differential average fluence for energies tested in this article: 3.3, 5.7, 9.7, and 13.8 MeV, with the respective differential average fluence ratio of 0.27:0.27:0.25:0.21. No shielding was considered. Left vertical scale: integrated fluence. Right vertical scale: differential fluence.

Therefore, these protons can reach the semiconductor detectors, through collimators, coded masks, and detector shielding, and cause damage to detector crystals and severe degradation of the γ-ray detector's performance during the mission lifetime, by deterioration of its charge transport properties [2].

We have been developing semiconductor-based γ-ray detection focal plane prototypes, namely CZT/CdTe detectors [6]–[9], [19]–[21], in a framework of high-energy astrophysics mission proposals, such as AMEGO [22]. In order to improve future missions' instrument inflight operational performances, we have recently studied and analyzed the proton radiation damage effects and the nuclear activation on a 2.0-mm-thick ACRORAD ohmic CdTe detector [23], induced by a single monochromatic proton beam with ≈14 MeV. The results showed a good CdTe detector radiation hardness for equivalent orbital environment proton fluences in a LEO [18].

Several previous studies on proton-induced radiation damage on CdTe detectors were carried out at several proton beam energies, fluxes, and fluences [24]–[29].

Herein, we evaluated the proton radiation damage effects on two 1.0-mm-thick EURORAD ohmic CdTe detectors, using a low MeV range proton radiation field, ensuring the protons are completely stopped along with the crystals' depth. The CdTe detectors were exposed to several irradiation sets with four proton beam energies at the Coimbra University ICNAS cyclotron: ≈13.8, ≈9.7, ≈5.7, and ≈3.3 MeV, for cumulative fluences from $\sim 2 \times 10^9$ up to $\sim 5 \times 10^{10}$ protons cm^{-2}.

With this proton irradiation sequence, we aimed to simulate the typical LEO proton almost-flat energy spectrum profile (Fig. 1) in the low-energy band, 3–14 MeV. The total fluence was tuned to generate a total proton fluence equivalent to ∼1, ∼2, ∼10, and ∼20 years in a LEO. Moreover, the proton beam irradiation sets with energies up to 14 MeV are fairly representative of the overall proton space environment, since the LEO trapped proton fluence is higher for the lower energy part of the trapped proton spectrum (Fig. 1) and the cumulative deleterious effects may be of much higher intensity, since the dose deposited per fluence unit is much higher than that deposited by protons with energy >16 MeV (average range >1.0 mm).

The proton radiation hardness in CdTe was analyzed by measuring the effects of the proton radiation field (3.3 up to 13.8 MeV), as the dose was increased, on the charge transport properties, namely the mobility-lifetime product for electrons $(\mu\tau)_e$, and holes $(\mu\tau)_h$, on the energy resolution and on the peak-to-valley ratio for up to 662 keV γ-rays.

II. Experimental Setup and Methodology

A. Detectors and Methods

The studied prototypes were 1.0-mm-thick EURORAD ohmic CdTe monolithic detectors with two different configurations: $5.0 \times 3.0 \times 1.0$ mm^3 (detector C) and $5.0 \times 2.0 \times 1.0$ mm^3 (detector H). The ohmic contacts were made of platinum electrodes (Pt/CdTe/Pt) with ∼80-nm thickness, without a guard ring around the readout electrode.

The detectors' output signals were processed by an electronic chain composed of a Canberra 2003BT charge preamplifier (sensitivity: 0.45 V/pC), a Tennelec TC243 amplifier (from 1- to 12-μs shaping time), and an ORTEC Maestro multichannel analyzer (MCA). The detectors were biased through the irradiated top electrode by a Canberra 3106D HV-power supply and the readout electrode was grounded via the preamplifier.

The two CdTe detectors were mounted on individual boards inside aluminum shielded boxes with radiation windows delimited by Ø2.0-mm Pb collimators with 3.0-mm thickness.

The CdTe detectors were irradiated and operated at room temperature (∼20 °C), matching the typical payload thermal operation conditions in the space orbit of the CdTe/CdZnTe detectors [30], [31]. Nevertheless, irradiation and operation at low temperatures, e.g., −170 °C, would allow evaluating with better sensitivity the effects of the variation in the defects (traps) concentration induced by proton irradiation in the CdTe crystal on mobility-lifetime products.

Scattering generated by defects dominates the mobility of electrons at low temperatures (<−120 °C), in contrast to the lattice scattering at room temperature. The overall hole mobility, which lowers with temperature decrease (<−50 °C), cannot be explained by the referred scattering mechanisms (which also fails to explain the electron mobility for temperatures <−150 °C); however, trap-controlled mobility could explain the observed behaviors [32]. Moreover, the carrier lifetime decreases for lower temperatures, given the more effective influence of traps (defects) on the carriers—the lower thermal velocity of the carriers allows longer interaction times—resulting in the capture of carriers. Typically, the mobility-lifetime products exhibit a reduction as the temperature decreases.

The measurement of the CdTe mobility-lifetime product for electrons $(\mu\tau)_e$ and holes $(\mu\tau)_h$ was carried out by the alpha-particle technique [33]. The detectors were irradiated

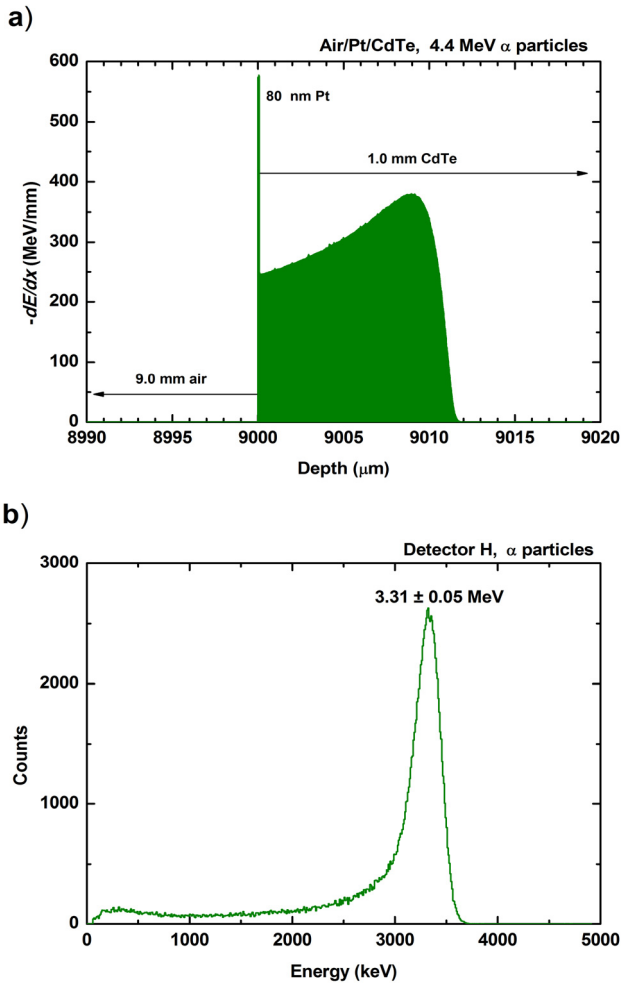

Fig. 2. (a) Energy loss per unit length of 4.4-MeV alpha particles within 9.0-mm air followed by an 80-nm Pt layer and 1.0-mm thick CdTe crystals, computed with the SRIM/TRIM toolkit [34]. (b) Alpha-particle energy spectrum measured with the detector H, at a bias voltage $V_{\text{bias}} = -140$ V and 1-μs shaping time.

by an ^{241}Am alpha-particle beam shaped by a Ø1.5-mm Cu collimator with 0.6-mm thickness. The 5.5-MeV alpha-particle source delivered ≈4.4 MeV alphas at the output of the source cover foil. Then, the alpha particle beam crossed ≈9.0 mm of air, until it strikes the CdTe 80-nm Pt electrode.

The energy deposited by the alpha-particles within the CdTe crystals was estimated with the SRIM/TRIM toolkit [34], being ≈3.4 MeV for an average range ≈11 μm, ensuring the formation of electron–hole pairs nearby the irradiated electrode, as shown in Fig. 2(a). This value is confirmed by the energy spectrum measured with the detector H, [Fig. 2(b)], using the electron induced signals, yielding ≈3.31 ± 0.05 MeV, considering the energy calibration error.

The $(\mu\tau)_e$ and $(\mu\tau)_h$ products were obtained by recording the alpha-particle pulse-height spectra at increasing bias voltage with opposite polarity among electrons and holes, where in each case single polarity carriers contribute to the signal development in the detector.

The spectroscopic properties of the CdTe detectors were evaluated when irradiated by several radioactive

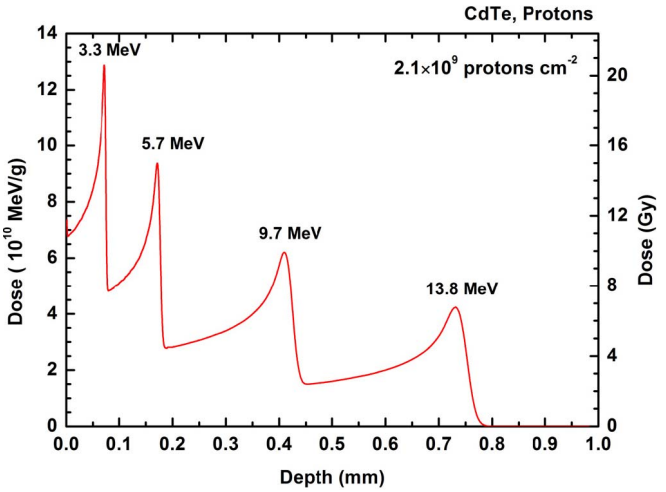

Fig. 3. Total dose deposited within a 1.0-mm thick CdTe crystal, by equal fluence proton beams of 3.3, 5.7, 9.7, and 13.8 MeV, versus depth. The dose was calculated from the stopping power curves computed with the SRIM/TRIM simulation toolkit [34]. The total fluence is 2.1×10^9 protons cm^{-2}, equivalent to a one-year mission.

sources: ^{241}Am (59.5 keV), ^{133}Ba (81 keV and 356 keV), ^{22}Na (511 keV), and ^{137}Cs (662 keV). An energy calibration protocol was implemented for both CdTe detector systems before and after each proton irradiation set.

For the γ-ray energy spectra, Gaussian fits were applied to the photopeaks selected (59.5, 356, 511, and 662 keV) allowing the measurement of the energy resolution [full-width at half-maximum (FWHM)] and the peak-to-valley ratio. The latter was obtained from the ratio of peak height to the average height on the lower energy side at 3σ from the peak centroid [26], [35]. The average height was calculated with five energy channels around the 3σ value equivalent to ∼8 keV energy range.

The peak-to-valley ratio might be a good indicator to quantify the peak's tail structure (peak's asymmetry) and the contribution of the deficient charge collection efficiency (CCE) for spectral degradation. It is valid when the FWHM (σ) is almost constant, and thus the relative position of the "valley" until it begins a tangible variation of the FWHM values. For other cases, the peak-to-valley ratio values could be contradictory with what would be expected due to the CCE behavior.

The time-frame of the irradiation experiment was ∼18 h for each CdTe detector, from irradiation set #1 (see Section II-B). Each irradiation set lasted for ∼30 min, then the detector was removed from the cyclotron bunker and connected to the power supply and the electronic readout chain. The detector was then biased at a low bias voltage, and the alpha-particle measurements started ∼30 min after the end of the irradiation set and lasted for ∼1.5 h. Next, the γ-ray spectral measurements were performed for ∼1.5 h.

Afterward, the detector was again setup in the cyclotron and the irradiation set #2 started within ∼30 min from the last time point. The remaining steps were performed as described above, until the end of irradiation set #4 and the respective alpha-particle and γ-ray spectral measurements.

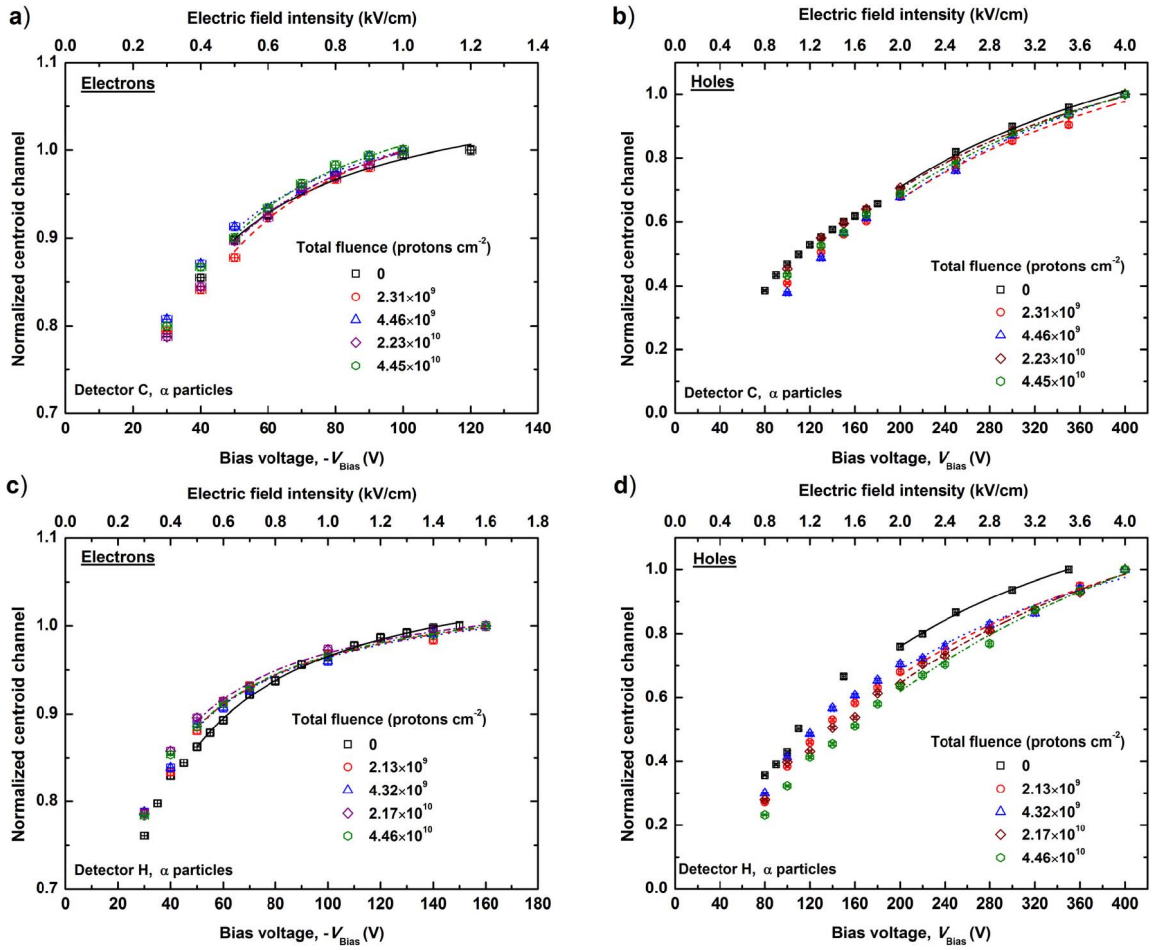

Fig. 4. Normalized alpha-particle peak centroid channel versus bias voltage measured for (a) and (c) electrons and (b) and (d) holes with increasing total proton fluence in detectors C and H. Lines: the Hecht fits applied to the selected data.

Systematic measurements of the leakage currents, versus the bias voltage, were performed in the two CdTe detectors before irradiation and after the proton maximum dose applied. A few additional values of leakage currents, in-between some irradiation sets, were also measured at the bias voltage of spectroscopic measurements, $V_{\text{bias}} = -140$ V.

B. Proton Irradiation Setup and Dose Deposited in CdTe

The proton radiation hardness tests were performed by exposing the CdTe detectors to four progressive irradiation sets—each set with protons beams from ≈13.8 down to ≈3.3 MeV—with cumulative fluences from $\sim 2 \times 10^9$ up to $\sim 5 \times 10^{10}$ protons cm^{-2}. The current direct proton beam with ≈13.8 MeV was degraded by the use of several thin degrader foils interleaved between the computer-controlled shutter and the CdTe detectors: 500-μm Al, 375-μm Nb, and 1000-μm Al, for the output proton energy of ≈9.7, ≈5.7, and ≈3.3 MeV, respectively. The energy of the proton beam after the degrader foils was estimated using a SRIM/TRIM toolkit [34]. Details of the ICNAS cyclotron proton irradiation setup can be found in [23] and [36]. The proton beam was Ø2.0 mm collimated.

During each irradiation set, the CdTe crystal was irradiated sequentially, with similar time lapses, at similar proton fluxes ($\sim 10^8$ protons cm^{-2}s^{-1}) by four proton beam energies: ≈13.8, ≈9.7, ≈5.7, and ≈3.3 MeV. The irradiation fluence applied to detector C during irradiation sets #1, #2, #3, and #4 was $\approx 0.23 \times 10^{10}$, $\approx 0.22 \times 10^{10}$, $\approx 1.8 \times 10^{10}$, and $\approx 2.2 \times 10^{10}$ protons cm^{-2}, respectively. The accumulated total fluence was $\approx 0.23 \times 10^{10}$, $\approx 0.45 \times 10^{10}$, $\approx 2.2 \times 10^{10}$, and $\approx 4.5 \times 10^{10}$ protons cm^{-2}, respectively, equivalent to ∼1.1, ∼2.1, ∼10.5, and ∼21.5 years in the LEO. The values applied to detector H were similar.

A set of simulations was performed with the SRIM/TRIM toolkit [34] to compute the stopping power curves for the proton beams of 3.3, 5.7, 9.7, and 13.8 MeV along with the CdTe crystals' depth, obtaining the following average ranges ≈0.07, ≈0.17, ≈0.42, and ≈0.75 mm, respectively. From these data, we have calculated the total dose deposited along with the crystals' depth, considering equal fluence for the four proton beams yielding a total fluence of 2.1×10^9 protons cm^{-2}, equivalent to a 1-year mission (Fig. 3).

As is expected, the total dose decreases with the depth, in addition to the local Bragg peaks of each proton beam energy. Furthermore, the local average and peaking doses were: ≈13 and ≈21 Gy; ≈9.3 and ≈15 Gy; ≈6.0 and ≈10 Gy; ≈3.2 and ≈6.9 Gy, while the average total dose was ≈5.9 Gy along 0.81-mm CdTe depth. Therefore, for higher energies,

any effects that might deteriorate the detector performances w impact the detector in-depth, instead of being concentrated near tl detector surface, as in the case of lower proton beam energies.

We should highlight that with proton energies lower tha 14 MeV, many of the nuclear reactions (p, xn) for $x \geq 2$ neutron with the natural isotopes of Cd and Te, are not initiated due to tl higher energy thresholds [23]. The nuclear activation reaction cross sections are strongly dependent the proton energy above the (p, n) reaction thresholds (rang 1–6 MeV), showing a sequence of maximum and minimu as other competitive nuclear reaction channels such as (p, 2r (p, 3n), etc., come into play. But for energy >50 MeV, whe the orbit differential average fluence also initiates a sharp decreas as shown in Fig. 1, the cross sections start decreasing steadily ar become very low for the energy of a few hundre of MeV.

Thus, we can infer that the 14–50 MeV energy band will pla some additional role in the nuclear activation, and th in γ -ray background and neutron damage effects within the CdT crystal.

III. Experimental Results

A. Mobility-Lifetime Products

To quantify the mobility-lifetime products, $(\mu\tau)_e$ and $(\mu\tau)_h$, alpha-particle pulse-height spectra were measured at increasing bias voltages. The electron-hole pairs are generated near the irradiated CdTe crystal surface; therefore, one charge carrier type is immediately collected by the irradiated electrode, while the other charge carrier drifts toward the opposite electrode, potentially crossing the entire crystal thickness until it is collected. Thus, the charge signal induced on the readout electrode is generated exclusively by the drift of the electrons (or holes) [37], [38].

The alpha-particle pulse-height (centroid channel, Ch) for a single charge carrier was measured versus the bias voltage, V_{bias}. The data were fit with a single charge carrier Hecht equation [33]:

$$\text{Ch} = A V_{\text{Bias}} \left[1 - \exp\left(-\frac{B}{V_{\text{Bias}}} \right) \right] \tag{1}$$

with $A = m(N_0 e(\mu\tau)_{e,h}/d^2)$ and $B = (d^2/(\mu\tau)_{e,h})$, where N_0 is the number of electron-hole pairs generated by the alpha-particle, e is the electron charge, d the CdTe detector thickness, $(\mu\tau)_{e,h}$ the mobility-lifetime product of electrons or holes, and m the charge to MCA channel conversion factor. The $(\mu\tau)_e$ and $(\mu\tau)_h$ were then estimated from the B parameter of (1) with $d = 1.0$ mm. In (1), V_{bias} should be read as the module of the bias voltage.

The Hecht equation assumes a uniform charge collection at a constant electric field in a parallel-plate detector. At a low bias voltage, the uniformity of the electric field is poor [38], thus the measurements should be taken at higher bias voltages for the low $(\mu\tau)_{e,h}$ material, $<10^{-3}$ cm^2 V^{-1}, as in this experiment. Additionally, at a low bias voltage, the pulse-height is not proportional to the induced total charge on the readout electrode at different bias voltages, due to the excessive charge pulse rise-time compared with the amplifier shaping-time, resulting in a variation of ballistic deficit due to the variation in the pulse rise-time—the net result is the underestimation of the $(\mu\tau)_{e,h}$ magnitudes.

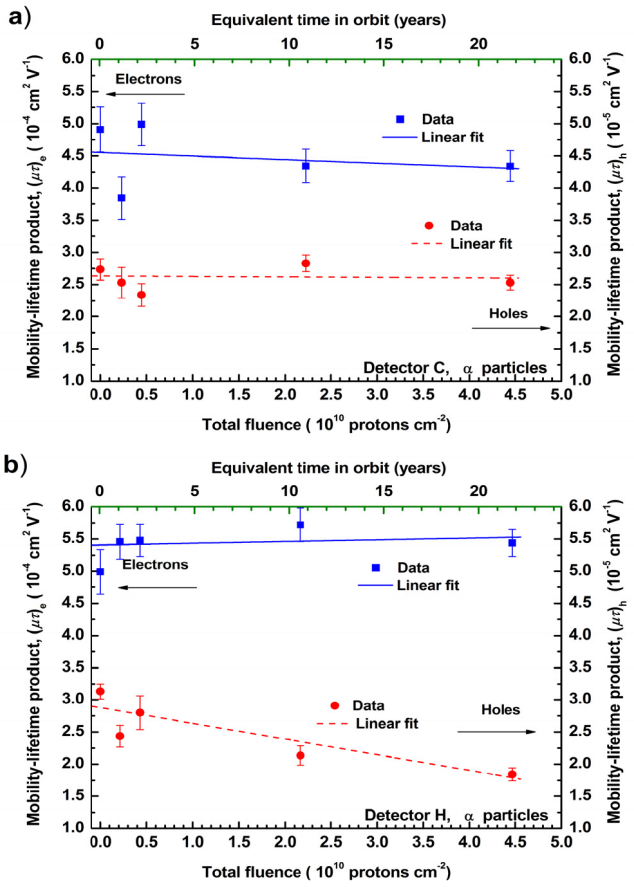

Fig. 5. Estimated values for electron and hole mobility-lifetime products versus the total proton fluence, in detectors (a) C and (b) H. The lines depicted represent the linear fits applied to each data set. Detector C: slope $(-0.055 \pm 0.116) \times 10^{-14}$ and $(-0.0072 \pm 0.0538) \times 10^{-15}$ cm^2 V^{-1}/protons cm^{-2}, respectively. Detector H: slope $(0.026 \pm 0.059) \times 10^{-14}$ and $(-0.24 \pm 0.06) \times 10^{-15}$ cm^2 V^{-1}/protons cm^{-2}, respectively.

We evaluated the charge (electrons or holes) drift times, in detector H, via the analysis of alpha-particle charge pulse rise-time, for electrons or holes, at charge preamplifier output with a digital oscilloscope. From these drift times, we estimated the amplifier shaping-time values to use and to read the "full" signal induced by electrons or holes. We could also estimate the carrier mobilities, if a significant proportion of the charge carriers, produced by the alpha-particle, drifts across the entire thickness of the CdTe detector [39].

Electron pulse rise times of ~150 and ~80 ns were measured at $V_{\text{bias}} = -50$ V and $V_{\text{bias}} = -100$ V, respectively, while hole pulse rise times of ~1000 and ~400 ns were measured at $V_{\text{bias}} = 100$ V and $V_{\text{bias}} = 200$ V, respectively. Therefore, at $V_{\text{bias}} = \pm 100$ V, the rough estimation of the electron mobility μ_e and the hole mobility μ_h was $\sim 1.3 \times 10^3$ cm^2 V^{-1} s^{-1} and $\sim 1.0 \times 10^2$ cm^2 V^{-1} s^{-1}, respectively. These figures are in accordance with those previously reported for CdTe material [40]. Thus, the amplifier shaping-time selected was 1 μs for electrons and 12 μs for holes.

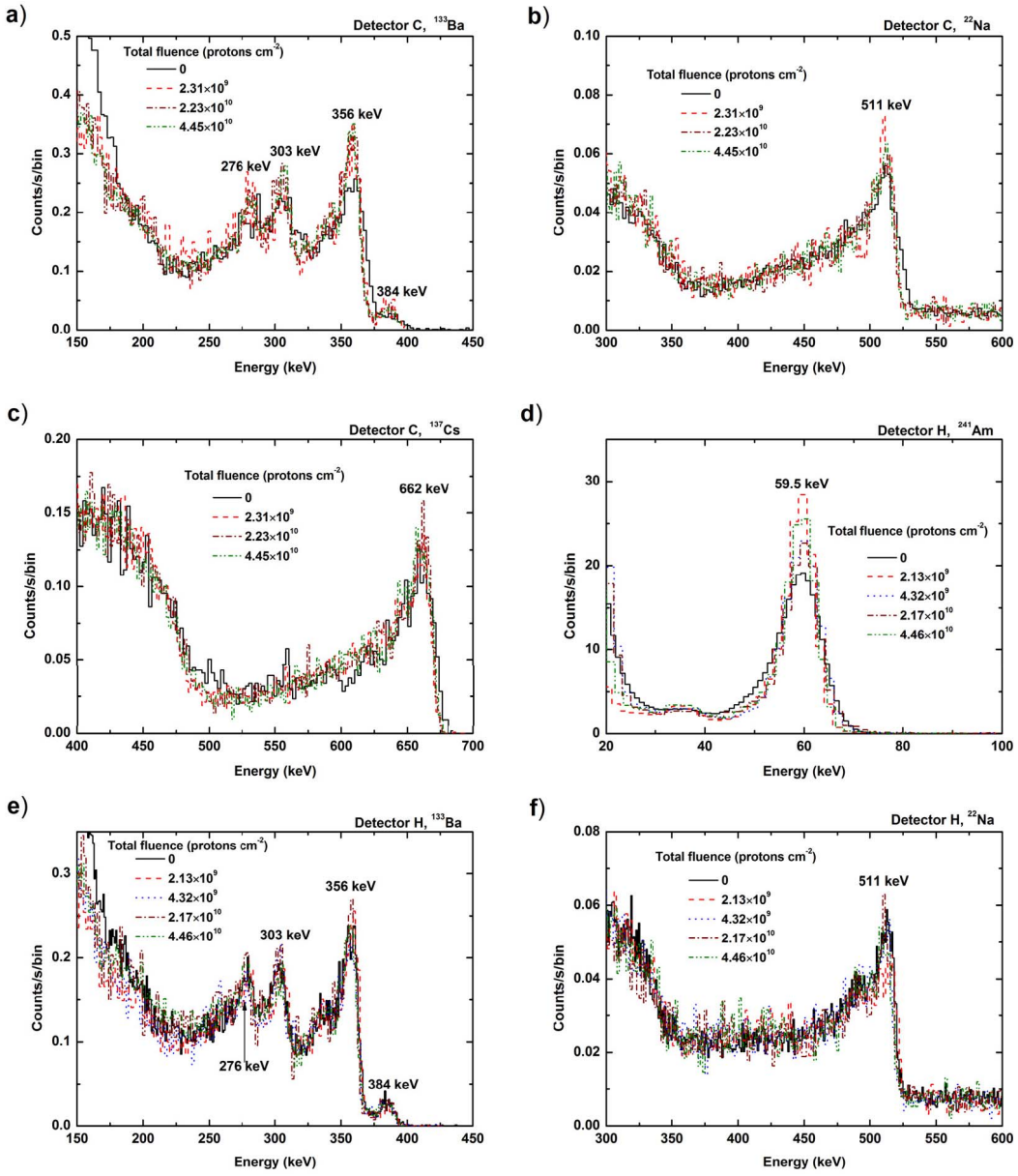

Fig. 6. γ-ray energy spectra obtained at increasing total proton fluence with the CdTe detectors. Detector C: (a) ^{133}Ba, exposure time—10^3, 5×10^2, 6×10^2, and 9×10^2 s, respectively; (b) ^{22}Na, exposure time—10^3, 1.6×10^3, 1.9×10^3, and 1.4×10^3 s, respectively; and (c) ^{137}Cs, exposure time—10^3, 5×10^2, 1.5×10^3, and 9×10^2 s, respectively. Detector H: (d) ^{241}Am, exposure time—9×10^2, 2×10^2, 10^2, 10^2, and 2×10^2 s, respectively; (e) ^{133}Ba, exposure time—9×10^2, 6×10^2, 6×10^2, 4×10^2, and 10^3 s, respectively; and (f) ^{22}Na, exposure time—9×10^2, 2.4×10^3, 2.4×10^3, 1.6×10^3, and 2×10^3 s, respectively. $V_{\text{bias}} = -140$ V and 1-μs shaping time.

The alpha-particle pulse-height versus the bias voltage, V_{bias}, is depicted in Fig. 4. The Hecht fits applied to the data series (with $V_{\text{bias}} \geq 50$ V and $V_{\text{bias}} \geq 200$ V, for electrons and holes, respectively, to minimize the ballistic deficit effects in the $(\mu\tau)_{e,h}$ values) yielded minimum reduced χ^2 [41] within ~0.4–2 range and ~0.7–4 range, respectively.

Fig. 5 represents $(\mu\tau)_{e,h}$ versus total proton fluence in each detector. In detector C, the $(\mu\tau)_e$ and $(\mu\tau)_h$ lie between 3.8×10^{-4} and 5.0×10^{-4} cm^2 V^{-1}, and between 2.3×10^{-5} and 2.8×10^{-5} cm^2 V^{-1}, respectively. Furthermore, the data show a small decrease of the $(\mu\tau)_e$ and $(\mu\tau)_h$ values, ~10% and ~7%, respectively, for a total proton fluence of ≈4.45×10^{10} protons cm^{-2} compared with no proton irradiation.

Moreover, linear fits applied to the data demonstrated that the variation in $(\mu\tau)_e$ and $(\mu\tau)_h$ was uncorrelated ($R^2 = 0.078$ and $R^2 = 0.006$, respectively) with the total proton fluence. Nevertheless, from the returned slopes (which are not significant at the 95% level [41]), we may extract the upper-limit of $(\mu\tau)_e$ and $(\mu\tau)_h$ proton fluence sensitivities: $\sim2\times10^{-15}$ cm^2 V^{-1}/protons cm^{-2} and $\sim6\times10^{-17}$ cm^2 V^{-1}/protons cm^{-2}, respectively.

In detector H, the $(\mu\tau)_e$ and $(\mu\tau)_h$ lie between 5.0×10^{-4} and 5.7×10^{-4} cm^2 V^{-1} and between 1.8×10^{-5} and 3.1×10^{-5} cm^2 V^{-1}, respectively. The data show an increase of ~10% in $(\mu\tau)_e$ and a decrease of ~40% in $(\mu\tau)_h$ for a total proton fluence of ≈4.46×10^{10} protons cm^{-2} compared

with no proton irradiation. Furthermore, a linear fitting to the data demonstrated that the variation in $(\mu\tau)_e$ and $(\mu\tau)_h$ was, respectively, uncorrelated ($R^2 = 0.25$) and correlated ($R^2 = 0.84$), with the total proton fluence. Based on the returned slope for electrons (which is not significant at the 95% level), the extracted upper-limit of $(\mu\tau)_e$ proton fluence sensitivity was $\sim 9 \times 10^{-16}$ cm^2 V^{-1}/protons cm^{-2}, while with the returned slope for holes (which is significant at the 95% level, $t = -3.9$, $p = 0.03$ [41]), the extracted upper-limit of $(\mu\tau)_h$ proton fluence sensitivity was $\sim 3 \times 10^{-16}$ cm^2 V^{-1}/ protons cm^{-2}.

B. Spectroscopic Properties

In order to analyze the effects of the proton radiation field on spectroscopic properties of the CdTe detectors as the total proton fluence increases, several spectra were collected, before and after each irradiation set with different γ-ray sources for a bias voltage, $V_{\text{bias}} = -140$ V and 1-μs shaping time. Between irradiation sets, the radioactive sources were positioned and centered accurately above the detector radiation window, ensuring constant distance and orientation during the measurements.

The spectra obtained for each γ-ray source for increasing total fluence values, up to $\approx 4.5 \times 10^{10}$ protons cm^{-2}, are depicted in Fig. 6. All the γ-ray spectra were scaled to the exposure time and to the energy bin, resulting in an easy inspection of the variations in-between the full-energy peaks for the same γ-ray line (detector C: 356, 511, and 662 keV; detector H: 59.5, 356, and 511 keV). The spectra present two relevant characteristics that differentiate the two detectors: the higher noise at C and the appearance of the small escape peak within 23–27 keV at the left of the main peaks at H.

The original pulse-height spectra (before applying the energy calibration) do not show a measurable peak shift toward lower energies, neither a progressive intensification of the peak's tail for increasing total proton fluence.

The energy resolution of several γ-ray lines shown in Fig. 6 versus the total proton fluence is depicted in Fig. 7. In detector C [Fig. 7(a)], the energy resolution at 356, 511, and 662 keV lies between 4.5 and 7.1%, 3.6 and 4.7%, and 2.9 and 3.4%, respectively, for a total proton fluence of up to $\approx 4.5 \times 10^{10}$ protons cm^{-2}. The respective peak-to-valley ratio is within 2.0 ± 0.2. For a total proton fluence of $\approx 4.5 \times 10^{10}$ protons cm^{-2} compared with no proton irradiation, the results show an overall improvement in the energy resolution of $\sim$35%, $\sim$15%, and $\sim$8%, respectively. The overall improvement in the peak-to-valley ratio was $\sim$30% at 662 keV, while at 356 and 511 keV the improvement/deterioration observed was $<$5%.

For a total proton fluence of up to $\approx 4.5 \times 10^{10}$ protons cm^{-2}, the energy resolution of detector H [Fig. 7(b)] at 59.5, 356, and 511 keV lies, respectively, between: 12.0% and 16.3%; 3.1 and 4.0%; and 2.5 and 3.2%. The measured peak-to-valley ratio is within 6.5 ± 1.5, 1.8 ± 0.2, and 1.6 ± 0.1, respectively. As for the total fluence of $\approx 4.5 \times 10^{10}$ protons cm^{-2} compared with no proton irradiation, the results show an overall improvement in the energy resolution of $\sim$25% at 59.5 keV, while at 356 and 511 keV, the improvement/deterioration observed was $<$5%. The overall improvement in the peak-to-valley ratio was $\sim$40% at 59.5 keV, while at 356 and 511 keV, the improvement/deterioration observed was $<$5%.

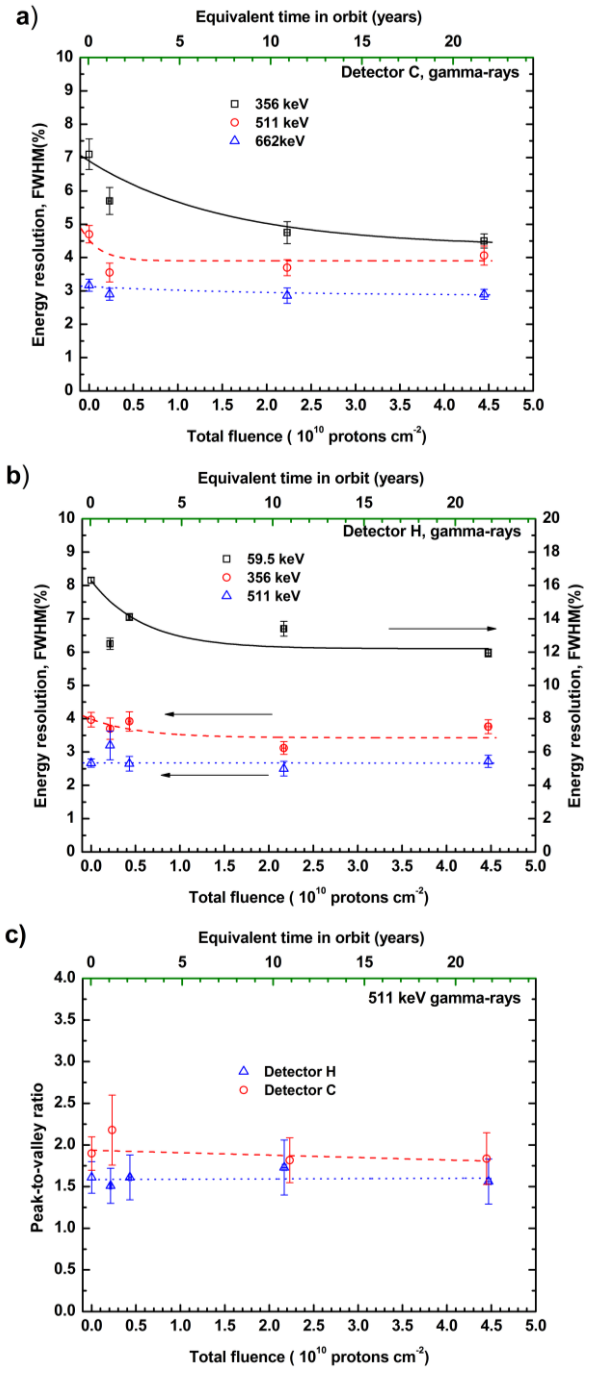

Fig. 7. Energy resolution versus the total proton fluence for several γ-ray lines with the CdTe detectors. (a) Detector C. (b) Detector H. Lines: the exponential decay fits applied to the data, just for guideline purposes. (c) Peak-to-valley ratio for the 511-keV line versus the total proton fluence, with detectors C and H. Lines: the linear fits applied to the data. $V_{\text{bias}} = -140$ V and 1-μs shaping time.

Exponential decay fits were applied to the energy resolution data, showing that the detectors' energy resolution response to the total proton fluence (or total dose) varies sharply

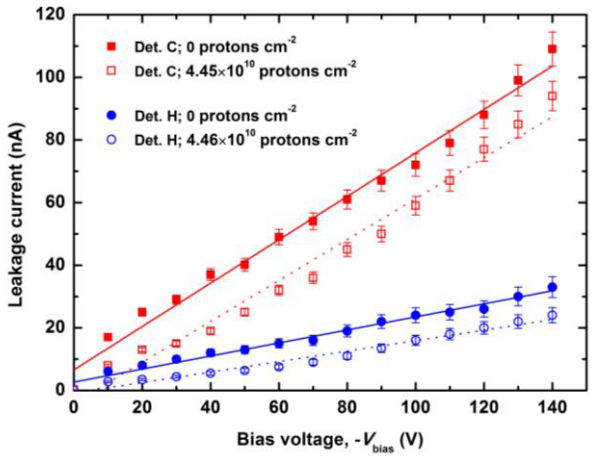

Fig. 8. Leakage current versus the bias voltage, measured with the detectors C and H at room temperature, before irradiation and after the maximum proton dose applied. From the slope of linear fits applied to the data, the resistivities of the two CdTe crystals, before and after irradiation, were calculated. Detector C: $(2.2\pm0.1)\times10^9$ and $(2.3\pm0.1)\times10^9$ Ω cm. Detector H: $(4.8\pm0.2)\times10^9$ and $(6.0\pm0.3)\times10^9$ Ω cm.

initially (this effect is more visible at lower energy γ-ray lines), up to $\sim5\times10^9$ protons cm^{-2}, almost saturating until the maximum total proton fluence applied in the experiment, $\approx4.5\times10^{10}$ protons cm^{-2}, is achieved.

In Fig. 7(c) is depicted the peak-to-valley ratio for the 511 keV line versus the total proton fluence, with detectors C and H, where we observed that its variation was uncorrelated with the total proton fluence, obtaining $R^2 = 0.24$ and $R^2 = 0.008$, respectively. For the 662 and 59.5 keV γ-ray lines, we observed that the variation of the peak-to-valley ratio was poorly correlated with the total proton fluence, $R^2 = 0.61$ and $R^2 = 0.40$, for detectors C and H, respectively. But, this variation (increase) is due to the improvement of the electronic noise and not of the CCE (see Section III-A).

IV. Discussion and Conclusion

In this article, we tested the proton radiation hardness of two CdTe crystals with moderate quality charge transport properties: mobility-lifetime products of $\sim5\times10^{-4}$ cm^2 V^{-1} and $\sim3\times10^{-5}$ cm^2 V^{-1}, for electrons and holes, respectively.

The two crystals exhibited low proton fluence (dose) sensitivity—the upper-limit of $(\mu\tau)_e$ and $(\mu\tau)_h$ sensitivity was $\sim2\times10^{-15}$ cm^2 V^{-1}/protons cm^{-2} ($\sim7\times10^{-7}$ cm^2 V^{-1}/Gy) and $\sim3\times10^{-16}$ cm^{2}V^{-1}/protons cm^{-2} ($\sim1\times10^{-7}$ cm^2 V^{-1}/Gy), respectively.

The measured $(\mu\tau)_{e,h}$ products exhibit values very close to the initial ones, prior to proton irradiation, with small variation (<10%) which was uncorrelated with the proton dose, except for holes in detector H that exhibited a steady decrease of the $(\mu\tau)_h$ value showing a reduction of ∼40% for a total fluence of $\approx4.5\times10^{10}$ protons cm^{-2} compared with no proton irradiation.

This reduction may confirm changes in the crystal lattice, possibly due to the increase of hole trap concentration, and/or change in spatial charge leading to a decrease of holes' lifetime, τ_h by a factor of ∼1.7. This assumption agrees with the estimates of hole mobility performed prior to the proton irradiation and after the final irradiation, in accordance with the ones described previously [40].

The small overall changes in $(\mu\tau)_{e,h}$ generate small changes in the energy resolution and the peak-to-valley ratio, beyond an initially sharp response up to $\sim5\times10^9$ protons cm^{-2}. This initial energy resolution improvement trend, also reported in [23], [25], and [26], may be explained by a reduction of the leakage current (as observed in Fig. 8 with the two detectors), probably due to the production of additional charge carrier traps in the forbidden energy gap leading to a reduction of electronic noise in detectors. A similar effect was reported in CdTe detectors [43]. Therefore, we can infer that the proton dose applied was not enough to modify significantly the charge transport properties and the spectroscopic properties of the detectors, due to the low perturbation of the steady-state of trap concentration [26], [27].

In conclusion, the findings in this article have their major impact on the long-time LEO mission of ∼20 years, and may be of great interest to other missions—short or medium lifetimes—crossing a more intense proton radiation field.

The low MeV range of proton radiation field (3.3–13.8 MeV) used in this study is potentially more relevant in the context of damage intensity than the medium and high MeV range, due to the presence of Bragg peaks inside the 1.0-mm-thick crystal. Indeed, the low MeV range may be more representative of the LEO proton radiation field to study the proton damage effects on 1.0-mm-thick CdTe detectors.

In this experiment, a high dose is delivered at a high dose rate, in very short time periods (few minutes at an interval of several hours), while in a real mission, the same dose will be delivered to the CdTe detectors during several years up to 20 years. Furthermore, shielding of the detectors must be considered, since it influences the proton spectrum profile—shift to lower energy with the reduction of differential fluence for low energies. Yet, the incident proton fluence on the detectors depends on the scientific instrumentation payload, on the use of shielding elements and their spatial arrangement, and on the different proton orientation angles in orbit.

The present study is important in the framework of the development of a CdTe instrument for a medium energy γ-ray observatory [9], [22], anticipating the possibility of its future launch in a LEO.

Finally, the use of γ-ray instrumentation based on CdTe detectors may reduce the LEO mission's cost-to-lifetime ratio provided by its fine expected lifetime, due to its high proton radiation hardness, and by its lower dependence of expensive proton shielding systems.

Acknowledgment

The author would like to thank the ICNAS Cyclotron Facility, Coimbra University, for their hospitality.

References

[1] J. M. Lavigne *et al.*, "The INTEGRAL experiment," *Nucl. Phys. B-Proc. Supplements*, vol. 60, no. 3, pp. 69–79, 1998.
[2] P. Leleux *et al.*, "Neutron-induced nuclear reactions and degradation in germanium detectors," *Astron. Astrophys.*, vol. 411, no. 1, pp. L85–L90, 2003.

[3] R. Terrier *et al.*, "In-flight calibration of the ISGRI camera," *Astron. Astrophys.*, vol. 411, no. 1, pp. L167–L172, 2003.

[4] M. Ajello *et al.*, "Cosmic X-ray background and earth albedo spectra with Swift BAT," *Astrophys. J.*, vol. 689, no. 2, p. 666, 2008.

[5] F. A. Harrison *et al.*, "The nuclear spectroscopic telescope array (NuSTAR) high-energy X-ray mission," *Astrophys. J.*, vol. 770, no. 2, p. 103, 2013.

[6] R. M. Curado da Silva, E. Caroli, S. del Sordo, and J. M. Maia, "Cadmium (Zinc) telluride 2D/3D spectrometers for scattering polarimetry," in *Semiconductor Radiation Detectors: Technology and Applications*, S. Reza and K. Iniewski, Eds. Boca Raton, FL, USA: CRC Press, 2017, pp. 241–282.

[7] E. Caroli *et al.*, "Hard X-ray and soft gamma ray polarimetry with CdTe/CZT spectro-imager," *Galaxies*, vol. 6, no. 3, p. 69, 2018.

[8] J. Knödlseder *et al.*, "GRI: Focusing on the evolving violent universe," *Exp. Astron.*, vol. 23, no. 1, pp. 121–138, 2009.

[9] M. Moita *et al.*, "Compton polarimetry with a multi-layer CdTe focal plane prototype," *Nucl. Instrum. Methods Phys. Res. A, Accel. Spectrom. Detect. Assoc. Equip.*, vol. 918, pp. 93–98, Feb. 2019.

[10] A. A. Moiseev, "Gamma-ray large area space telescope: Mission overview," *Nucl. Instrum. Methods Phys. Res. A, Accel. Spectrom. Detect. Assoc. Equip.*, vol. 588, nos. 1–2, pp. 41–47, Apr. 2008.

[11] N. Gehrels *et al.*, "The Swift gamma-ray burst mission," *Astrophys. J.*, vol. 611, no. 2, p. 1005, 2004.

[12] R. P. Lin *et al.*, "The reuven ramaty high-energy solar spectroscopic imager (Rhessi)," in *The Reuven Ramaty High-Energy Solar Spectroscopic Imager (RHESSI)*, R. P. Lin, B. R. Dennis, and A. O. Benz, Eds. Dordrecht, The Netherlands: Springer, 2003, pp. 3–32.

[13] C. Winkler *et al.*, "The INTEGRAL mission," *Astron. Astrophys.*, vol. 411, no. 1, pp. L1–L6, 2003.

[14] A. Poghosyan and A. Golkar, "CubeSat evolution: Analyzing CubeSat capabilities for conducting science missions," *Prog. Aerosp. Sci.*, vol. 88, pp. 59–83, Jan. 2017.

[15] E. R. Benton and E. V. Benton, "Space radiation dosimetry in low-Earth orbit and beyond," *Nucl. Instrum. Methods Phys. Res. B, Beam Interact. Mater. At.*, vol. 184, nos. 1–2, pp. 255–294, 2001.

[16] G. P. Ginet *et al.*, "AE9, AP9 and SPM: New models for specifying the trapped energetic particle and space plasma environment," *Space Sci. Rev.*, vol. 179, nos. 1–4, pp. 579–615, 2013.

[17] T. Takahashi, K. Mitsuda, and R. Kelley, "The ASTRO-H mission," in *CP1248, X-Ray Astronomy-2009: Present Status, Multi-Wavelength Approach and Future Perspectives*, A. Comastri, M. Cappi, and L. Angelini, Eds. College Park, MD, USA: American Institute of Physics, 2010, pp. 537–542.

[18] (2016). *OMERE 4.2*. [Online]. Available: http://www.trad.fr/en/space/omere-software/

[19] S. Antier *et al.*, "Hard X-ray polarimetry with Caliste, a high performance CdTe based imaging spectrometer," *Exp. Astron.*, vol. 39, no. 2, pp. 233–258, 2015.

[20] R. M. Curado da Silva *et al.*, "Polarimetric performance of a Laue lens gamma-ray CdZnTe focal plane prototype," *J. Appl. Phys.*, vol. 104, no. 8, Aug. 2008, Art. no. 084903.

[21] R. M. Curado da Silva *et al.*, "Polarization degree and direction angle effects on a CdZnTe focal plane performance," *IEEE Trans. Nucl. Sci.*, vol. 59, no. 4, pp. 1628–1635, Aug. 2012.

[22] A. Moiseev, "All-sky medium energy gamma-ray observatory (AMEGO)," in *Proc. 35th Int. Cosmic Ray Conf.*, 2018, vol. 798, pp. 1–8.

[23] N. Simões *et al.*, "Inflight proton activation and damage on a CdTe detection plane," *Nucl. Instrum. Methods Phys. Res. A, Accel. Spectrom. Detect. Assoc. Equip.*, vol. 887, pp. 183–191, Jan. 2018.

[24] F. Lebrun *et al.*, "ISGRI: A CdTe array imager for INTEGRAL," *Proc. SPIE*, vol. 2806, Oct. 1996, Art. no. 253985.

[25] L. A. Franks *et al.*, "Radiation damage measurements in room-temperature semiconductor radiation detectors," *Nucl. Instrum. Methods Phys. Res. A, Accel. Spectrom. Detect. Assoc. Equip.*, vol. 428, no. 1, pp. 95–101, 1999.

[26] M. Zanarini *et al.*, "Radiation damage induced by 2 MeV protons in CdTe and CdZnTe semiconductor detectors," *Nucl. Instrum. Methods Phys. Res. B, Beam Interact. Mater. At.*, vol. 213, pp. 315–320, Jan. 2004.

[27] B. Fraboni, A. Cavallini, N. Auricchio, and M. Bianconi, "Deep traps induced by 700 keV protons in CdTe and CdZnTe detectors," *IEEE Trans. Nucl. Sci.*, vol. 54, no. 4, pp. 828–833, Aug. 2007.

[28] O. Limousin *et al.*, "ASTRO-H CdTe detectors proton irradiation at PIF," *Nucl. Instrum. Methods Phys. Res. A, Accel. Spectrom. Detect. Assoc. Equip.*, vol. 787, pp. 328–335, Jul. 2015.

[29] Y. Eisen, L. G. Evans, S. Floyd, C. Schlemm, R. Starr, and J. Trombka, "Radiation damage of Schottky CdTe detectors irradiated by 200 MeV protons," *Nucl. Instrum. Methods Phys. Res. A, Accel. Spectrom. Detect. Assoc. Equip.*, vol. 491, nos. 1–2, pp. 176–180, 2002.

[30] F. Lebrun, "The ISGRI CdTe gamma camera in-flight behavior," in *Proc. IEEE Symp. Conf. Rec. Nucl. Sci.*, Rome, Italy, Oct. 2004, pp. 4373–4377.

[31] S. D. Barthelmy *et al.*, "The burst alert telescope (BAT) on the SWIFT midex mission," *Space Sci. Rev.*, vol. 120, nos. 3–4, pp. 143–164, 2005.

[32] K. Suzuki, S. Seto, T. Sawada, and K. Imai, "Carrier transport properties of HPB CdZnTe and THM CdTe:Cl," *IEEE Trans. Nucl. Sci.*, vol. 49, no. 3, pp. 1287–1291, Jun. 2002.

[33] H. Chen *et al.*, "Characterization of large cadmium zinc telluride crystals grown by traveling heater method," *J. Appl. Phys.*, vol. 103, no. 1, 2008, Art. no. 014903.

[34] F. Ziegler, M. D. Ziegler, and J. P. Biersack, "SRIM—The stopping and range of ions in matter (2010)," *Nucl. Instrum. Methods Phys. Res. B, Beam Interact. Mater. At.*, vol. 268, nos. 11–12, pp. 1818–1823, 2010.

[35] J. M. Maia, R. M. Curado da Silva, and Y.-S. Kim, "Prospects on low-Z elements K fluorescence and actinide-radionuclides L fluorescence X-ray detection with cooled CZT," *IEEE Trans. Nucl. Sci.*, vol. 62, no. 2, pp. 577–587, Apr. 2015.

[36] S. Ghithan *et al.*, "Development of a PET cyclotron based irradiation setup for proton radiobiology," *J. Instrum.*, vol. 10, no. 2, 2015, Art. no. P02010.

[37] Z. He, G. F. Knoll, and D. K. Wehe, "Direct measurement of product of the electron mobility and mean free drift time of CdZnTe semiconductors using position sensitive single polarity charge sensing detectors," *J. App. Phys.*, vol. 84, no. 10, p. 5566, 1998.

[38] A. E. Bolotnikov *et al.*, "Use of the drift-time method to measure the electron lifetime in long-drift-length CdZnTe detectors," *J. Appl. Phys.*, vol. 120, no. 10, 2016, Art. no. 104507.

[39] P. J. Sellin, A. W. Davies, A. Lohstroh, M. E. Ozsan, and J. Parkin, "Drift mobility and mobility-lifetime products in CdTe:Cl grown by the travelling heater method," *IEEE Trans. Nucl. Sci.*, vol. 52, no. 6, pp. 3074–3078, Dec. 2005.

[40] A. Owens and A. Peacock, "Compound semiconductor radiation detectors," *Nucl. Instrum. Methods Phys. Res. A, Accel. Spectrom. Detect. Assoc. Equip.*, vol. 531, nos. 1–2, pp. 18–37, 2004.

[41] P. R. Bevington and D. K. Robinson, *Data Reduction and Error Analysis for the Physical Sciences*, 3rd ed. New York, NY, USA: McGraw-Hill, 2003.

[42] G. F. Knoll, *Radiation Detection and Measurement*, 4th ed. Hoboken, NJ, USA: Wiley, 2010.

[43] G. H. Nakano, W. L. Imhof, and J. R. Kilner, "Effects of 33-MeV proton bombardent on the performance of CdTe Gamma-ray detectors," *IEEE Trans. Nucl. Sci.*, vol. NS-23, no. 1, pp. 467–472, Feb. 1976.